A finite volume method with linearisation in time for the solution of advection-reaction-diffusion systems

Jayantha Pasdunkorale Arachchige[a1 2] and Graeme J. Pettet[b]

Mathematical Sciences School, Queensland University of Technology, Brisbane, Australia
E-mail: [a]j.pasdunkoralearachige@qut.edu.au, [b]g.pettet@qut.edu.au

Abstract

The numerical solution in one space dimension of advection–reaction–diffusion systems with nonlinear source terms may invoke a high computational cost when the presently available methods are used. Numerous examples of finite volume schemes with high order spatial discretisations together with various techniques for the approximation of the advection term can be found in the literature.

Almost all such techniques result in a nonlinear system of equations as a consequence of the finite volume discretisation especially when there are nonlinear source terms in the associated partial differential equation models.

This work introduces a new technique that avoids having such nonlinear systems of equations generated by the spatial discretisation process when nonlinear source terms in the model equations can be expanded in positive powers of the dependent function of interest.

The basis of this method is a new linearisation technique for the temporal integration of the nonlinear source terms as a supplementation of a more typical finite volume method. The resulting linear system of equations is shown to be both accurate and significantly faster than methods that necessitate the use of solvers for nonlinear system of equations.

Keywords: Nonlinear, Reaction, Advection, Diffusion, Shock, Chemotaxis, Finite volume method

1. Introduction

The use of advection-reaction-diffusion (ARD) equations for modelling biological processes can provide insight and perspective into the development of complex yet robust behaviour in living systems, that otherwise is difficult to achieve by direct or indirect observation of a living system. As a result, there exists now a substantial and increasing body of literature dealing

[1]Corresponding author. Alternative e-mail addresses: jayantha@maths.ruh.ac.lk, jayantha64@gmail.com
[2]On sabbatical leave from Department of Mathematics, University of Ruhuna, Matara, Sri Lanka.

with mathematical models of phenomena as diverse as tumour growth and invasion [1], the movement of cells in tissues [2] and pattern formation [3].

Usually the transport component of such models are dominantly diffusive or dominantly advective but there is a developing interest in problems where the contribution of both processes is important as indeed are the magnitudes of the reaction terms [4]. Although some traction in determining the behaviour of such systems may be gained by examining them at diminishing limits of diffusion or advection, the numerical solution of the full system can prove problematic. Such is the case for the mathematical models of embryologic development [5] where the system smoothly makes the transition from being dominantly parabolic, exhibiting smooth-fronted travelling waves, to dominantly hyperbolic with shock-fronted travelling waves. Typically the methods adopted to reliably capture the travelling wavefronts in such models employ flux-limiting or gradient averaging techniques at the front [4].

Here we introduce a new method for numerically solving such ARD systems in one space dimension, based on the usual finite volume paradigm [6] with a third order upwinding scheme [7] for the calculations of the advection term in space and by employing a very effective integral approximation technique in time for chosen nonlinear reaction terms. This temporal integration approximation has been used in finite element and finite difference methods for solving partial differential equations where source term linearisation is required, see for example [8] and [9]. We find that the use of this linearisation technique in a finite volume method for solving the problems of our interest has been very effective in terms of computational cost for the simulations. We illustrate how the numerical scheme is implemented for a class of multi-species partial differential equation models where the diffusion component of each balance equation is taken to be Fickian and the advective velocity depends upon the gradient of another species. Such models are typically used in the description of chemotactic phenomena where cellular invasion is directed by a diffusive attractant [4, 5]. We also demonstrate the effectiveness of the method described here by resolving a number of recent example models within this domain of advection–reaction–diffusion systems.

These models usually conform to the following description of two (or more) interacting species $u(x,t)$ and $c(x,t)$ say, both of which disperse by a process modelled as Fickian diffusion. Additionally species $u(x,t)$, usually taken to be a population density of some cellular species in time t at position x, is being advectively transported with a velocity determined by the gradient of another species $c(x,t)$. As a generic example of such systems we will take the following equations to hold for $0 < x < L < \infty$ and $t > 0$;

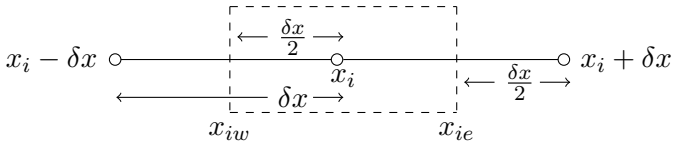

(a) An interior control volume.

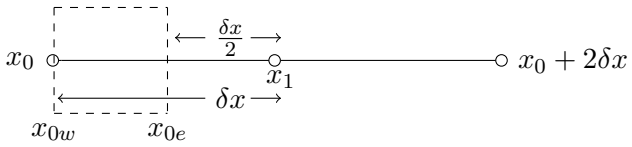

(b) A boundary control volume.

Figure 1: Interior and boundary control volumes.

$$\frac{\partial u}{\partial t} = D_u \frac{\partial^2 u}{\partial x^2} - \frac{\partial}{\partial x}\left(u\chi(c)\frac{\partial c}{\partial x}\right) + f(u,c) \tag{1}$$

$$\frac{\partial c}{\partial t} = D_c \frac{\partial^2 c}{\partial x^2} + h(u,c) \tag{2}$$

where $f(u,c)$ and $h(u,c)$ describe the reaction between the species, and D_u and D_c are diffusion coefficients. The function $\chi(c)$ describing the sensitivity of the cells to the chemotactic signal is variously taken to be a constant or a nonlinear function of c, for example $\chi(c) = \kappa$, $\chi(c) = 1/(1+\kappa c)$ or $\chi(c) = \kappa c^2 - \kappa c + 1$ where κ is a constant [10]. Initial and boundary conditions may be generally represented as appropriate.

Although we are considering here only one dimensional systems involving 2 or 3 species, the methods described naturally extend to higher dimensional problems with more species.

2. Discretisation of equations using Finite Volume Method

The model equations are discretised using the vertex centered control volume method with a uniform mesh. The nodes, $x_i = i\delta x,\ i = 0, 1, 2, 3, ..., N$, are chosen along the $x-$axis between $x = x_0 = 0$ and $x = x_N = L$; where $N\delta x = L$. Control volumes are constructed around the interior nodes with control volume faces at $x_{iw} = x_i - \frac{\delta x}{2}$ and $x_{ie} = x_i + \frac{\delta x}{2}$ for $i = 1, 2, 3, ..., N-1$ as shown in Figure 1(a). At the ends of the domain $[0, \frac{\delta x}{2}]$ and $[L - \frac{\delta x}{2}, L]$, see Figure 1(b), are considered as the boundary control volumes.

Integration of equation (1) over the control volume $[x_{iw}, x_{ie}] = [x_i - \dfrac{\delta x}{2}, x_i + \dfrac{\delta x}{2}]$ w.r.t. x gives the following equation:

$$\frac{\partial}{\partial t}\left(\int_{x_{iw}}^{x_{ie}} u\,dx\right) = D_u\left[\frac{\partial u}{\partial x}\right]_{x_{iw}}^{x_{ie}} - \left[u\chi(c)\frac{\partial c}{\partial x}\right]_{x_{iw}}^{x_{ie}} + \int_{x_{iw}}^{x_{ie}} f(u,c)\,dx$$

The above equation can be approximated as follows under suitable assumptions:

$$\begin{aligned}\frac{\partial}{\partial t}\left(U_i\delta x\right) \simeq D_u&\left(\frac{U_{i+1}-U_i}{\delta x}-\frac{U_i-U_{i-1}}{\delta x}\right)\\ &-\left(U_{ie}\chi(C_{ie})\frac{C_{i+1}-C_i}{\delta x}-U_{iw}\chi(C_{iw})\frac{C_i-C_{i-1}}{\delta x}\right)\\ &+f(U_i,C_i)\delta x;\end{aligned}$$

where $U_i = U_i(t) \simeq u(x_i,t)$ and $C_i = C_i(t) \simeq c(x_i,t)$. Here, the values of C at control volume faces can be approximated by using the values of C at the nodes around each control volume face, for example, $C_{ie} \simeq \dfrac{C_i + C_{i+1}}{2}$.

2.1. A high order approximation of spatial integrals

It should be noticed that the linear approximations $\displaystyle\int_{x_{iw}}^{x_{ie}} u(x,t)\,dx \simeq U_i\delta x$ and $\displaystyle\int_{x_{iw}}^{x_{ie}} f\,dx \simeq f(U_i,C_i)\delta x$ above are made on the assumption that the function value at the centre of the control volume represents the average of the function within the control volume. This is not true for many diffusion problems. A higher order approximation of $\displaystyle\int_{x_{iw}}^{x_{ie}} u(x,t)\,dx$ can be considered by using the trapezoidal rule for integration and the Taylor series expansions of the function u around the point x_i as follows:

$$\begin{aligned}\int_{x_{iw}}^{x_{ie}} u\,dx &\simeq \frac{\delta x}{2}(u_{iw}+u_{ie}) - \frac{(\delta x)^3}{12}\left(\frac{\partial^2 u}{\partial x^2}\right)_\zeta;\quad x_{iw}<\zeta<x_{ie}\\ &\simeq \frac{\delta x}{2}\left[2U_i + \frac{(\delta x)^2}{4}\left(\frac{\partial^2 u}{\partial x^2}\right)_i\right] - \frac{(\delta x)^3}{12}\left(\frac{\partial^2 u}{\partial x^2}\right)_i\\ &= \frac{\delta x}{2}\left[2U_i + \frac{(\delta x)^2}{12}\left(\frac{\partial^2 u}{\partial x^2}\right)_i\right]\\ &\simeq \frac{\delta x}{2}\left[2U_i + \frac{(\delta x)^2}{12}\frac{U_{i-1}-2U_i+U_{i+1}}{(\delta x)^2}\right]\\ &= \frac{\delta x}{24}\left[U_{i-1}+22U_i+U_{i+1}\right].\end{aligned}$$

This result has been used in [6] which also explains the necessity of careful treatment of boundary conditions and requirement of suitable treatment for the advection term when this approximation is used for the discretisation of advection-reaction-diffusion equations.

For a boundary control volume, for example for the control volume $[0, \delta x/2]$, one may use the trapezoidal rule for approximating the above integral as follows:

$$\begin{aligned}\int_{x_0}^{\delta x/2} u\,dx &\simeq \frac{\delta x/2}{2}(u_0+u_{\delta x/2}) - \frac{(\delta x)^3}{12}\left(\frac{\partial^2 u}{\partial x^2}\right)_\zeta\\ &\simeq \frac{\delta x}{4}\left[U_0 + \frac{U_0+U_1}{2}\right]\\ &= \frac{\delta x}{8}\left[3U_0+U_1\right]\end{aligned}$$

due to the fact that a good approximation for $\left(\dfrac{\partial^2 u}{\partial x^2}\right)_\zeta;\ 0<\zeta<\delta x/2$ will not directly be available.

2.2. Approximation of advection term

One may use one of the different approximation methods from among the available techniques such as averaging, upwinding and flux limiting for the treatment of the advection term in order to replace the values of the governing function [4] at control volume faces during the process of finite volume discretisation.

The third order upwinding scheme that retains the second order derivative in the Taylor series expansion for approximation of the governing function at the control volume faces can be used in order to have an increased accuracy of the solution; see the QUICK scheme in [7]. This scheme leads to an approximation of, for example, U_{ie} by the following:

$$U_{ie} = \frac{1}{2}(U_{i+1} + U_i) - \frac{1}{8}(U_{i+1} - 2U_i + U_{i-1})$$

under the condition that the mass flow rate, say v, through the face is greater than zero. It is easy to show that

$$U_{ie} = \frac{1}{2}(U_{i+1} + U_i) - \frac{1}{8}(U_{i+2} - 2U_{i+1} + U_i)$$

when $v < 0$. Therefore one could approximate U_{ie} or U_{iw} using the following expressions with appropriate coefficients a_k and b_k:

$$U_{ie} = \sum_{k=i-1}^{i+2} a_k U_k \text{ or } U_{iw} = \sum_{k=i-2}^{i+1} b_k U_k,$$

respectively, in order to use the third order upwinding scheme for the discretisation.

Hence the spatial integration of the equation (1) over the interior control volume leads to the following when the above approximations are used.

$$\begin{aligned}\frac{\delta x}{24}\frac{\partial}{\partial t}(U_{i-1} + 22U_i + U_{i+1}) &= D_u\left(\frac{U_{i+1} - U_i}{\delta x} - \frac{U_i - U_{i-1}}{\delta x}\right) \\ &- \left[\left(\sum_{k=i-1}^{i+2} a_k U_k\right)\chi(C_{ie})\frac{C_{i+1} - C_i}{\delta x} - \left(\sum_{k=i-2}^{i+1} b_k U_k\right)\chi(C_{iw})\frac{C_i - C_{i-1}}{\delta x}\right] \\ &+ \frac{\delta x}{24}(f(U_{i-1}, C_{i-1}) + 22f(U_i, C_i) + f(U_{i+1}, C_{i+1})).\end{aligned}$$

The integration of the above equation over the time interval $[j\delta t, (j+1)\delta t]$ and its approx-

imation leads to

$$\begin{aligned}
&\frac{\delta x}{24}\left[\left(U_{i-1}^{(j+1)}+22U_i^{(j+1)}+U_{i+1}^{(j+1)}\right)-\left(U_{i-1}^{(j)}+22U_i^{(j)}+U_{i+1}^{(j)}\right)\right]\\
&=\frac{D_u}{\delta x}\left[\left(U_{i+1}^{(j+1)}-2U_i^{(j+1)}+U_{i-1}^{(j+1)}\right)(1-\alpha)\delta t+\left(U_{i+1}^{(j)}-2U_i^{(j)}+U_{i-1}^{(j)}\right)\alpha\delta t\right]\\
&-\left(\chi(C_{ie}^{(j+1)})\frac{C_{i+1}^{(j+1)}-C_i^{(j+1)}}{\delta x}\sum_{k=i-1}^{i+2}a_kU_k^{(j+1)}-\chi(C_{iw}^{(j+1)})\frac{C_i^{(j+1)}-C_{i-1}^{(j+1)}}{\delta x}\sum_{k=i-2}^{i+1}b_kU_k^{(j+1)}\right)(1-\alpha)\delta t\\
&-\left(\chi(C_{ie}^{(j)})\frac{C_{i+1}^{(j)}-C_i^{(j)}}{\delta x}\sum_{k=i-1}^{i+2}a_kU_k^{(j)}-\chi(C_{iw}^{(j)})\frac{C_i^{j}-C_{i-1}^{(j)}}{\delta x}\sum_{k=i-2}^{i+1}b_kU_k^{(j)}\right)\alpha\delta t\\
&+\frac{\delta x}{24}\sum_{k=i-1}^{i+1}\alpha_k\bar{f}(U_k^{(j)},U_k^{(j+1)},C_k^{(j)},C_k^{(j+1)},\beta)\delta t;
\end{aligned}\tag{3}$$

where $0\le\alpha,\beta\le 1$ and $\alpha_{i-1}=1,\alpha_i=22,\alpha_{i+1}=1$. Here $\bar{f}$ is a representative value for the function f for the interval $[j\delta t,(j+1)\delta t]$ as described below.

2.3. Time integration of nonlinear reaction terms

It should be noted that when the function $f(u,c)$ contains nonlinear terms of u, the above equation will end up with nonlinear terms of $U_i^{(j+1)}$ if traditional methods are used to approximate the integral $\int_{j\delta t}^{(j+1)\delta t} f(U_i,C_i)\,dt$. This situation is often handled by using methods available for example in [11] for solving nonlinear system of equations. However, such methods for the solutions of nonlinear systems of equations arising from more complicated cell migration problems lead to costly computational algorithms which are not suitable for some of the available solvers [12].

Therefore, in this work that introduces a new approach to reduce the above computational cost while maintaining the accuracy of the solution, the integral

$$\int_{j\delta t}^{(j+1)\delta t} f(U_i,C_i)dt\simeq\bar{f}(U_i^{(j)},U_i^{(j+1)},C_i^{(j)},C_i^{(j+1)},\beta)\delta t;\quad\text{where } 0\le\beta\le 1$$

is approximated appropriately so that $\bar{f}$ can be written as a linear function of U_i^{j+1} as follows:

$$\bar{f}(U_i^{(j)},U_i^{(j+1)},C_i^{(j)},C_i^{(j+1)},\beta)=\bar{f}_1(U_i^{(j)},C_i^{(j)},C_i^{(j+1)},\beta)U_i^{(j+1)}+\bar{f}_2(U_i^{(j)},C_i^{(j)},C_i^{(j+1)},\beta)\tag{4}$$

assuming that δt is sufficiently small to keep the accuracy of the approximation.

There are many ways for approximating an integration of a function on a very small interval. For example, one can use δt times the geometric average of the function values at the end points of the interval rather than using the arithmetic average of those values (or vice-versa) to approximate the integral of the function over the interval $[j\delta t,(j+1)\delta t]$. As an example, a

representative function of $U_i - U_i^2$ for a time point $t = (\overline{j+1} - \beta)\delta t$; $0 \leq \beta \leq 1$ of the time interval $[j\delta t, (j+1)\delta t]$ can be constructed as follows

$$\begin{aligned} U_i^{(j+1-\beta)} - \left(U_i^{(j+1-\beta)}\right)^2 &\simeq \beta U_i^{(j)} + (1-\beta)U_i^{(j+1)} - \left((U_i^{(j)})^2\right)^{\beta} \left((U_i^{(j+1)})^2\right)^{1-\beta} \\ &\simeq \beta U_i^{(j)} + (1-\beta)U_i^{(j+1)} - \left((U_i^{(j)})^{\beta}(U_i^{(j+1)})^{1-\beta}\right)^2 \\ &= \beta U_i^{(j)} + (1-\beta)U_i^{(j+1)} - (U_i^{(j)})^{2\beta}(U_i^{(j+1)})^{2(1-\beta)} \end{aligned}$$

by using the arithmetic average and the geometric average for linear and quadratic terms respectively.

One could easily notice that the above approximation represents $U_i(1-U_i)$ within the interval $[j\delta t, (j+1)\delta t]$ since it becomes $U_i^{(j+1)}(1-U_i^{(j+1)})$ and $U_i^{(j)}(1-U_i^{(j)})$ when $\beta = 0$ and $\beta = 1$, respectively. It gives an interesting and very useful result for finite volume discretisations of the problem of interest in this work when $\beta = \frac{1}{2}$ is used for a function in the form of $f(u,c) = (\mu_1 + \nu_1 c)u - \mu_2 u^2$ in equation (1) as follows:

$$\begin{aligned} f^{(j+\frac{1}{2})}(U_i, C_i) &= \left(\mu_1 U_i + \nu_1 C_i U_i - \mu_2 U_i^2\right)^{(j+\frac{1}{2})} \\ &\simeq \mu_1 \frac{U_i^{(j)} + U_i^{(j+1)}}{2} + \frac{\nu_1}{2}\left(C_i^j U_i^{(j)} + C_i^{(j+1)} U_i^{(j+1)}\right) - \mu_2 U_i^{(j)} U_i^{(j+1)} \\ &= \left(\frac{\mu_1}{2} + \frac{\nu_1}{2} C_i^{(j+1)} - \mu_2 U_i^{(j)}\right) U_i^{(j+1)} + \left(\mu_1 \frac{U_i^{(j)}}{2} + \frac{\nu_1}{2}\left(U_i^{(j)} C_i^{(j)}\right)\right); \end{aligned}$$

where the geometric mean of the quantities over the time interval is considered for the quadratic term U_i^2 and the arithmetic average is used directly for the linear terms U_i and $C_i U_i$ of the governing function $f(U_i, C_i)$. The above discretisation of f has the form given in equation (4).

It is straight forward to show that

$$\begin{aligned} \left(\int_{j\delta t}^{(j+1)\delta t} \{U(x_i,t)\}^2 dt\right) - U_i^{(j)} U_i^{(j+1)} \delta t = &\frac{(\delta t)^2}{2}\left(U_i^{(j+1)}\left(\frac{dU_i}{dt}\right)^{(j)} - U_i^{(j)}\left(\frac{dU_i}{dt}\right)^{(j+1)}\right) \\ &+ \frac{(\delta t)^3}{6}\left(U_i^{(j+1)}\left(\frac{d^2U_i}{dt^2}\right)^{(j)} + U_i^{(j)}\left(\frac{d^2U_i}{dt^2}\right)^{(j+1)}\right) \\ &+ ... \end{aligned}$$

if one uses the Taylor expansions of $U(x_i,t) = U(x_i, t_j + \delta t_1)$ and $U(x_i,t) = U(x_i, t_{j+1} - \delta t_2)$ around t_j and t_{j+1}, respectively, with $\delta t_1 = t - t_j$ and $\delta t_2 = t_{j+1} - t$ in order to integrate $\{U(x_i,t)\}^2 = U(x_i, t_j + \delta t_1)U(x_i, t_{j+1} - \delta t_2)$ over the time interval $[j\delta t, (j+1)\delta t]$. Note also that $\delta t = \delta t_1 + \delta t_2 = t_{j+1} - t_j$. This proves that the error in the approximation of $\int_{j\delta t}^{(j+1)\delta t} \{U(x_i,t)\}^2 dt$ by $U_i^{(j)} U_i^{(j+1)} \delta t$ is in the order of $(\delta t)^2$ for sufficiently small time step δt. This approach can be used to prove the accuracy in the approximation of $\int_{j\delta t}^{(j+1)\delta t} \{U(x_i,t)\}^m dt$ by $\left(U_i^{(j)}\right)^{(m-1)} U_i^{(j+1)} \delta t$ for any integer power $m \geq 2$. This will also enable linearisation of any

nonlinear function which can be expressed as a power series with non-negative powers of the function of interest.

2.4. Linearised finite volume equations

Equations (3) and (4) lead to the following implicit finite volume discretisation of equation (1) between the time interval $[j\delta t, (j+1)\delta t]$:

$$\sum_{k=i-2}^{i+2} p_k U_k^{(j+1)} = \sum_{k=i-2}^{i+2} q_k U_k^{(j)} + \sum_{k=i-1}^{i+1} r_k; \tag{5}$$

for interior control volumes[3] around the points x_i; $i = 1, 2, 3, ..., N-1$ (with $p_{-1} = q_{-1} = 0$ and $p_{N+1} = q_{N+1} = 0$) and $j = 0, 1, 2, 3, ..., m$ where the coefficients p_k, q_k and r_k depend on the function values $U_k^{(j)}$, $C_k^{(j)}$ and $C_k^{(j+1)}$ for $k = i-2, i-1, i, i+1, i+2$ and other parameters as shown in the Appendix.

For the simulations carried out here, the penta–diagonal system of equations given in equation (5) is reduced to a tri–diagonal system of equations in the form

$$\sum_{k=i-1}^{i+1} p_k U_k^{(j+1)} = -p_{i-2} U_{i-2}^{(j+1)} - p_{i+2} U_{i+2}^{(j+1)} + \sum_{k=i-2}^{i+2} q_k U_k^{(j)} + \sum_{k=i-1}^{i+1} r_k \tag{6}$$

by replacing the terms $U_{i-2}^{(j+1)}$ and $U_{i+2}^{(j+1)}$ in the right hand side with $U_{i-2}^{(j)} + \delta t \left[\frac{\partial U_{i-2}}{\partial t}\right]_j$ and $U_{i+2}^{(j)} + \delta t \left[\frac{\partial U_{i+2}}{\partial t}\right]_j$, respectively. The time derivatives of the function U can be approximated using the already calculated values of the dependent functions at time level j in finite difference form of the governing equation (1). This arrangement of explicit treatment of terms that are away from point x_i allows us to use a tri–diagonal matrix algorithm that significantly reduces the computational cost while maintaining the accuracy of the numerical solutions.

When an updated value for $C_i^{(j+1)}$ is not readily available it can be again approximated by

$$C_i^{(j+1)} = C_i^{(j)} + \delta t \left[\frac{\partial C_i}{\partial t}\right]_j$$

[3]Discretisation of the governing equation at the boundary control volumes, $[0, \frac{\delta x}{2}]$ and $[L - \frac{\delta x}{2}, L]$, is done making sure that the conservativity of the system is maintained considering the type of boundary conditions associated with the models simulated here. The finite volume method discussed here is applied for all of the coupled equations which are associated with diffusion, advection and reaction or any combination of them.

in the above approximations. The term $\left[\frac{\partial C_i}{\partial t}\right]_j$ can be calculated utilising the available values u and c at time level $j\delta t$ in the finite difference approximation of the partial differential equation associated with the function c. This approach avoids the appearance of the terms $C_i^{(j+1)}$ (or $U_i^{(j+1)}$) in the coefficients of $U_i^{(j+1)}$ (or $C_i^{(j+1)}$) when discretising equation (1) (or equation (2)).

It should also be noted that the discretisation technique discussed here can be used not only for the term $f(u,c)$ in equation (1) but also for other term $h(u,c)$ in equation (2) in order to obtain a similar approximation as follows:

$$\bar{h}(U_i^{(j)}, U_i^{(j+1)}, C_i^{(j)}, C_i^{(j+1)}, \beta) = \bar{h}_1(U_i^{(j)}, U_i^{(j+1)}, C_i^{(j)}, \beta) C_i^{(j+1)} + \bar{h_2}(U_i^{(j)}, U_i^{(j+1)}, C_i^{(j)}, \beta) \quad (7)$$

for discretising equation (2) in order to solve the equations simultaneously.

2.5. The advantage of having a linear system of equations

The above system of equations, together with finite volume equations relevant to boundary control volumes, can be solved directly in order to advance the solution forward a time step, δt. The approach discussed here has avoided the requirement of solving a nonlinear system of equations using a method such as an inexact Newton method as there are no nonlinear terms of the governing function u at time level $(j+1)\delta t$. It should be noted that the approach discussed here to integrate the reaction term in order to arrive at a linearised approximation can be easily extended to 2D and 3D problems. Analysis of other nonlinear functions together with Taylor approximations for those functions at the vicinity of each control volume will be helpful for linearising functions other than the quadratic function discussed here. The careful choice of β in the linearisation will also play an important role for such functions.

2.6. Calculation of spatial discretisation error in the absence of an exact solution

Since exact solutions are not available for most of the examples discussed here, the spatial discretisation error associated with the numerical solution is measured using a mass balance error (MBE), see for example [4], as follows:

$$\text{MBE} = \frac{1}{m-1} \sum_{k=1}^{m-1} \left[\frac{\int_0^L \left(u(x,t_{k+1}) - u(x,t_k)\right) dx}{t_{k+1} - t_k} - \left(\int_0^L F(x,t_{k+1}) dx - J(x,t_{k+1}) \Big|_0^L \right) \right]$$

where

$$J(x,t) = -D_u \frac{\partial u}{\partial x} + u\chi(c) \frac{\partial u}{\partial x} \text{ and } F(x,t_{k+1}) = f(u(x,t_{k+1}), c(x,t_{k+1}))$$

for equation (1). The integration required for the calculation of the MBE are approximated by, for example,

$$\int_0^L F(x,t_{k+1}) dx \simeq \sum_{i=1}^{N} F(x_i, t_{k+1}) \delta x_i$$

where $F(x_i, t_{k+1})$ are the numerical approximations of the function $F(x, t_{k+1})$ at the points x_i and the δx_i is the size of the control volume associated with x_i.

This error measurement, MBE that depends on time step size by definition, calculates the temporal average of the difference between the total change in each species in the domain of interest from one time step to the next, and the net production within the domain plus the net movement into the domain. The MBE calculated using the updated information at each time level is a measure derived to check for any error that will arise if the conservativity of the problem is violated by the spatial discretisation of the PDEs. We find that the MBE for the numerical simulations of the models discussed here is decreasing as the size of the control volumes (δx) are decreased along with proportional time steps (δt).

2.7. Method of manufactured solutions for code verification

In order to verify the accuracy of the numerical techniques used to generate solutions for a partial differential equation (PDE) model one can use the method of manufactured solutions [13, 14, 15] when there are no exact solutions known. This method provides a general procedure for generating an analytic solution for a new PDE model constructed from the model under investigation for the purpose of code accuracy verification. This approach is used here to illustrate the accuracy of the code used for the numerical simulations with the newly proposed method for solving advection–reaction–diffusion problems.

3. Numerical Simulations

The above finite volume method with linearisation (*FVML*) of the reaction term is used here for the numerical simulation of a variety of systems of ARD equations, employing the RK4 method for the solution of the ordinary differential equations that are associated with the model equations. Coupled equations are solved simultaneously using the updated solutions available at each time step.

A number of different one dimensional examples are provided here to illustrate the effectiveness of using the finite volume method discussed above which incorporates a new approach of arriving at a linear system of finite volume equations for nonlinear coupled system of PDEs.

In the first example, the solutions of an advection–diffusion problem which has an exact solution are depicted, allowing us to verify numerical solutions of an advection–dominated problem [4]. This example specifically illustrates the advantage of using a high order approximation for spatial integration together with a third order upwinding scheme for the approximation of the advection term at the control volume faces. Then we converted this problem into an ARD equation by introducing a nonlinear source term which is balanced by an equivalent explicit function

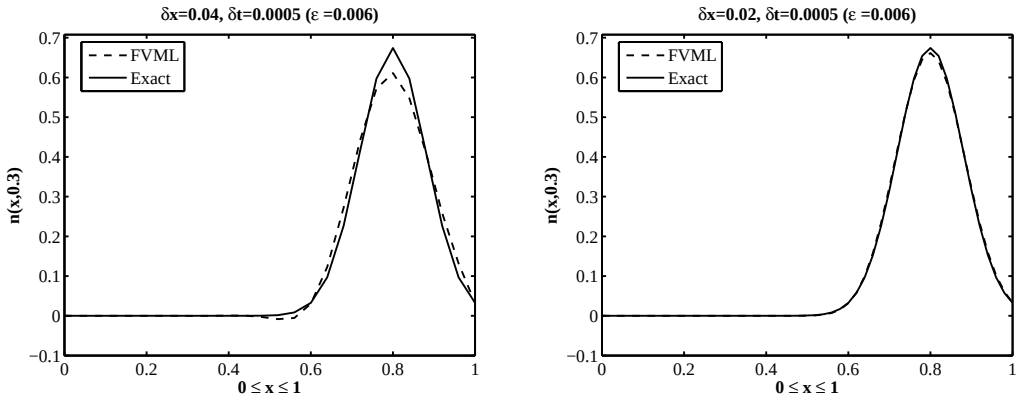

(a) (b)

Figure 2: Plot of exact solution (solid line) and numerical solution (dotted line) of equation (8) using a third order upwinding scheme with $\chi = 2$, $\epsilon = 0.006$ and $x_0 = 0.2$ for (a) 25 and (b) 50 control volumes with time step $\delta t = 0.0005$.

so that the equation still satisfy the same exact solution in order to test the FVML method introduced in this paper. This conversion helps us to verify the FVML code according to the method of manufactured solutions discussed in [13], [14] and [15]. The next example provides a benchmark exact solution for the assessment of the newly proposed linearisation technique on a reaction-diffusion problem. The equation associated with this problem is also converted to an ARD equation by introducing an advection term to test the FVML technique. Furthermore, in order to verify the numerical code the method of manufactured solutions is again used in the subsequent example. A further example shows the accuracy of the method when it is applied to a coupled advection–reaction–diffusion equation system with a nonlinear reaction term leading to solutions in the form of travelling waves. Finally an advection–reaction–diffusion problem with nonlinear reaction terms that often lead to oscillating numerical solutions on coarse meshes [4, 16] is considered. Further examples to illustrate the ability of the method to simulate advection–reaction–diffusion problems with nonlinear reaction terms where the solutions of interest exhibit shock-fronted travelling wave profiles will be discussed in the next article associated with this work.

Note. All the numerical simulations depicted here are done using Matlab codes on a desktop computer (2.99 GHz, 3.21 GB of RAM) running Matlab 7.9.0.529 (R2009b) 32-bit(win32).

3.1. Diffusion of wound healing chemoattractant

A non–dimensionalised advection–diffusion equation with analytic solution has been considered in [4] with different values for the diffusion coefficient of the chemoattractant species. The

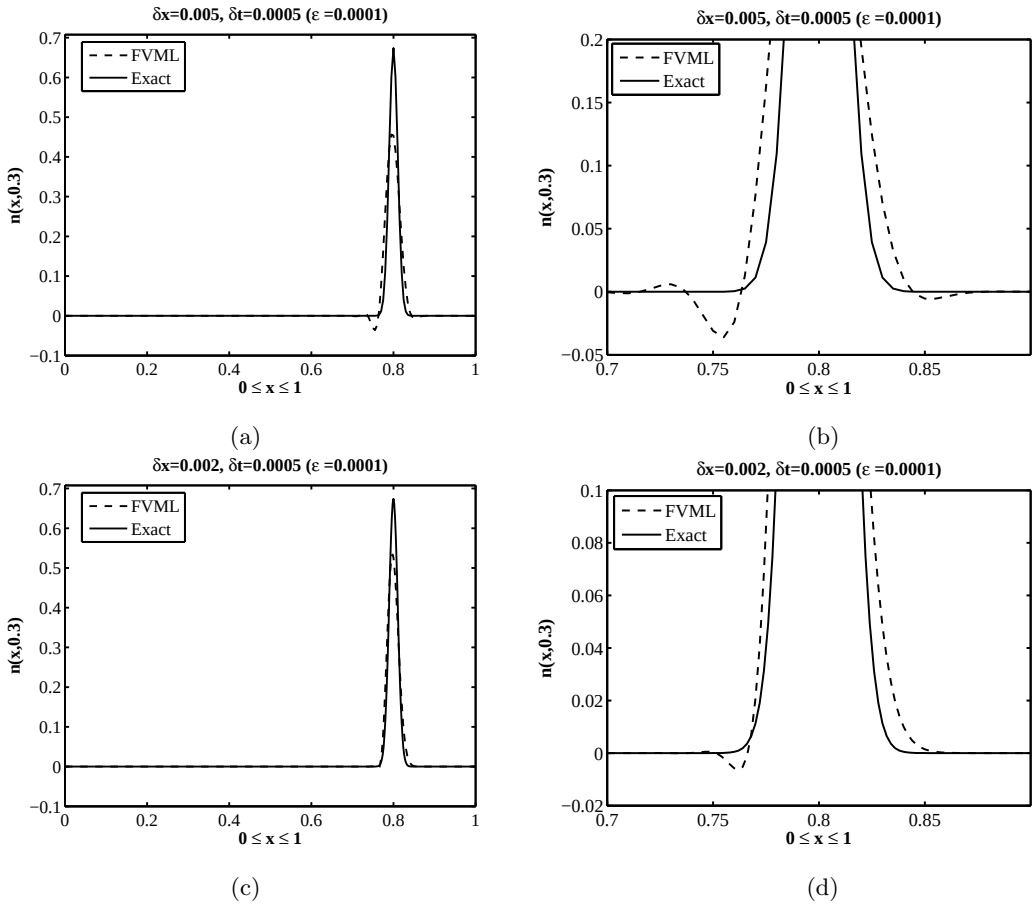

Figure 3: Plot of exact solution (solid line) and numerical solution (dotted line) of equation (8) using a third order upwinding scheme with $\epsilon = 0.0001$, $\chi = 2$ and $x_0 = 0.2$ for 200 control volumes ((a) and (b)) and 500 control volumes ((c) and (d)) with time step $\delta t = 0.0005$.

relevant model equation has the form

$$\frac{\partial n}{\partial t} - \frac{\partial}{\partial x}\left(\epsilon\frac{\partial n}{\partial x} - \chi n\right) = 0, \;\; 0 < x < 1, \; t > 0, \tag{8}$$

with boundary conditions

$$n(0,t) = \frac{1}{\sqrt{1+4t}} exp\left[-\frac{(x_0+\chi t)^2}{\epsilon(1+4t)}\right], \;\; t > 0,$$

$$n(1,t) = \frac{1}{\sqrt{1+4t}} exp\left[-\frac{(1-x_0-\chi t)^2}{\epsilon(1+4t)}\right], \;\; t > 0,$$

and initial condition

$$n(x,0) = exp\left[-\frac{(x-x_0)^2}{\epsilon}\right], \;\; 0 \le x \le 1.$$

These initial and boundary conditions had been chosen in [4] so that an exact closed form solution given by

$$n(x,t) = \hat{n}(x,t) = \frac{1}{\sqrt{1+4t}} exp\left[-\frac{(x-x_0-\chi t)^2}{\epsilon(1+4t)}\right]$$

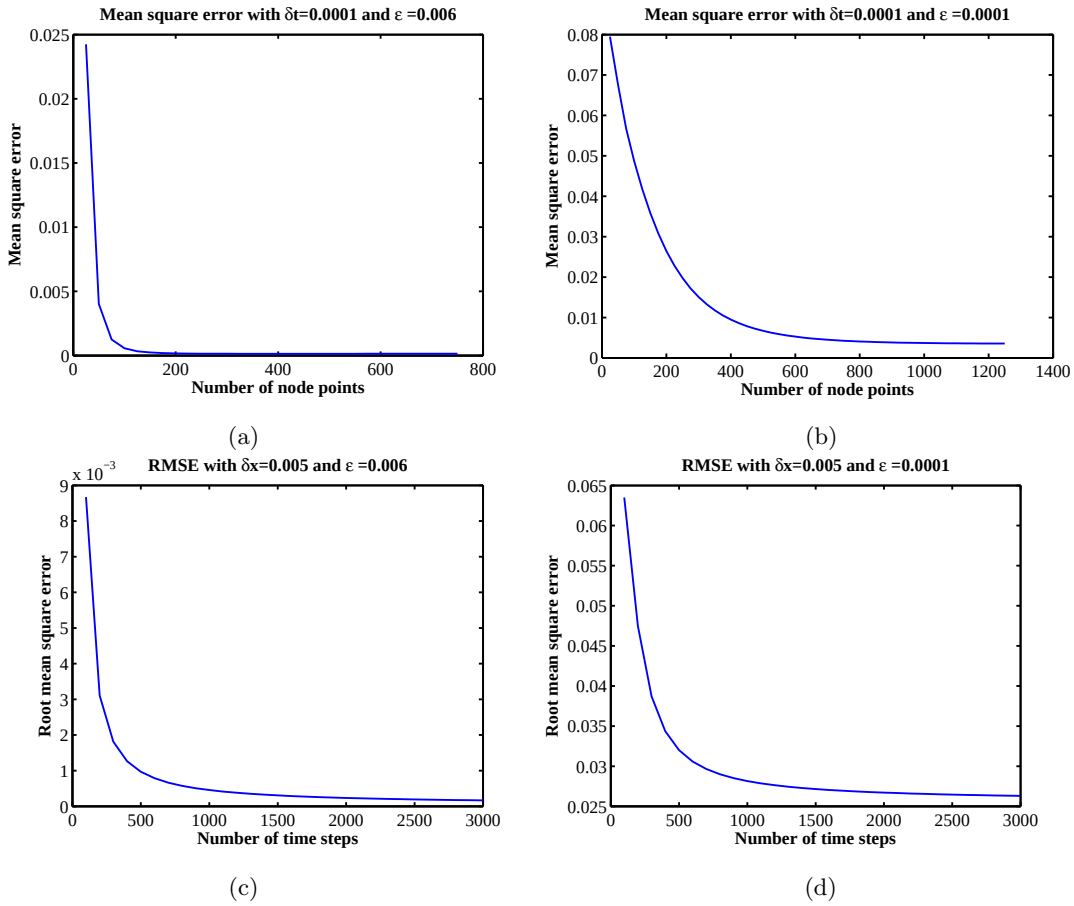

Figure 4: *Convergence of the solutions of equation (8) using a third order upwinding scheme with* $\chi = 2$ *and* $x_0 = 0.2$. *The convergence of RMSE as the number of node points changes for (a)* $\epsilon = 0.006$ *and* $\delta t = 0.0001$, *and (b)* $\epsilon = 0.0001$ *and* $\delta t = 0.0001$. *The convergence of RMSE as the number of time points changes for (c)* $\epsilon = 0.006$ *and* $\delta x = 0.005$, *and (d)* $\epsilon = 0.0001$ *and* $\delta x = 0.005$.

could be obtained.

Figures 2 and 3 provide the exact solution (solid line) and numerical solution (dotted line) obtained using finite volume technique (Crank-Nicholson scheme: $\alpha = 0.5$) with third order upwinding scheme to estimate the advective chemoattractant quantity for different diffusion coefficients and number of control volumes. It can be easily seen from Figure 2 that the numerical solution with just 50 control volumes with time step $\delta t = 0.0005$ avoids the negative solution near $x = 0.6$ that occurs when 25 control volumes are used for the simulation. This error occurs even with 100 control volumes when MATLAB's partial differential equation solver, `pdepe.m`, and the Numerical Algorithms Group routine, D03PCF, are used for this problem [4]. Figure 3 shows the necessity of increasing the number of control volumes and time steps according to the Péclet number associated with the problem when a very small diffusion coefficient is used. It should be noted that FVML recovers the spike in Figure 3b and agrees with the exact solution

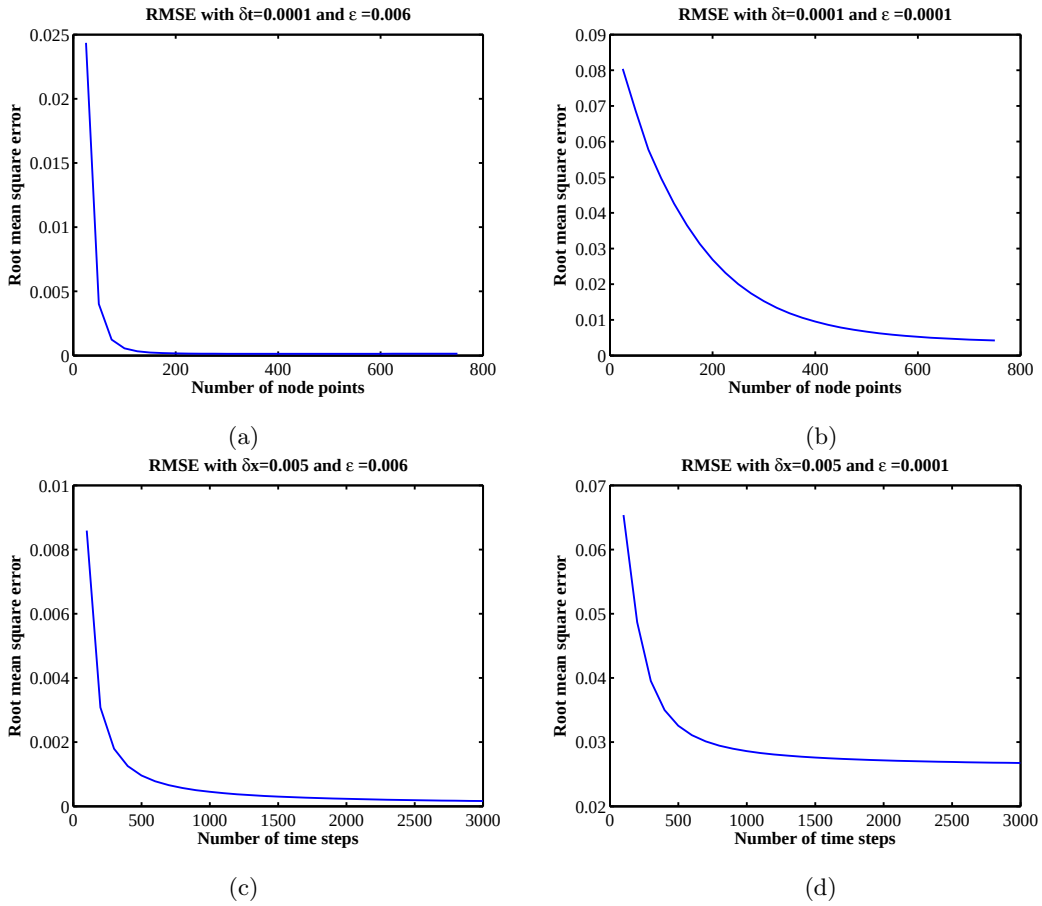

Figure 5: *Convergence of the solutions of equation (9) using a third order upwinding scheme with linearisation of source term (FVML) with* $\chi = 2$ *and* $x_0 = 0.2$. *The convergence of RMSE as the number of node points changes for (a)* $\epsilon = 0.006$ *and* $\delta t = 0.0001$, *and (b)* $\epsilon = 0.0001$ *and* $\delta t = 0.0001$. *The convergence of RMSE as the number of time points changes for (c)* $\epsilon = 0.006$ *and* $\delta x = 0.005$, *and (d)* $\epsilon = 0.0001$ *and* $\delta x = 0.005$.

when a very small time step and a space step are used for the simulations.

Figure 4 shows how the RMSE changes when the time step or the space step changed while one of them is fixed. These figures provide evidence of stability of the solutions obtained using the third order upwinding method discussed here.

We modify the advection–diffusion equation discussed here by adding a reaction term into the equation as shown below in order to verify the code with the FVML technique introduced here. We used the method of the manufactured solutions as described in [13], [14] and [15] to construct the problem which still satisfy the same exact solution. The modified equation is read as

$$\frac{\partial n}{\partial t} - \frac{\partial}{\partial x}\left(\epsilon\frac{\partial n}{\partial x} - \chi n\right) - n(1-n) = -g_1(x,t), \;\; 0 < x < 1, \; t > 0, \tag{9}$$

where $g_1(x,t)$ is explicitly given by $g_1(x,t) = \hat{n}(x,t)(1-\hat{n}(x,t))$ so that this modified partial

differential equation still satisfies the exact solution $n = \hat{n}(x,t)$ when the same initial and boundary conditions above are used. The results FVML code were in agreement with the exact solutions and the comparison of the convergence of the RMSE for different time steps and space steps are shown in the Figure 5 which again provides evidence of the stability of the method introduced.

3.2. A model of thermal wave propagation

Here we will simulate solutions of a thermal wave problem [8] which is associated with a time dependent heat equation with a nonlinear source term. This test problem has a smooth analytical solution [17] in the form of a propagating wave. The nonlinear reaction-diffusion equation is

$$\frac{\partial T}{\partial t} = \frac{\partial^2 T}{\partial x^2} + \frac{8}{\delta^2} T^2(1-T); \tag{10}$$

where $\delta > 0$ with boundary conditions $T(-\infty, t) = 1$ and $T(\infty, t) = 0$ and the initial condition $T(x,0) = 0.5(1 - \tanh(x/\delta))$. The analytic solution of this problem is

$$T(x,t) = \hat{T}(x,t) = \frac{1}{2}\left(1 - \tanh\left[\frac{x - 2t/\delta}{\delta}\right]\right) \text{ for } -\infty < x < \infty, \;\; t > 0.$$

Figure 6 depicts the comparison of the results obtained using `pdepe.m` and the proposed method with the exact solutions and Table 1 gives an indication of the computational time and relevant root mean squares error in generating these solutions. Interested reader will note that the FVML provides smaller RMSE than `pdepe.m` for all the cases except for the case with $\delta x = 0.02$ and $\delta t = 0.0005$. However, the high computational time ($450.1s$) required by `pdepe.m` suggests that `pdepe.m` has used a smaller time step than 0.0005 for this specific case. It is worthwhile to note that the RMSE values of FVML for $\delta t = 0.00005$ (or for $\delta x = 0.02$) decrease with δx (or δt). These results suggest that FVML requires the space step to be around $\delta x = 0.02$ and the time step to be around $\delta t = 0.00005$ for the convergence of the method, for this specific test problem considered with $\delta = 0.1$. Note that the parameter value $\delta = 0.1$ is used for simulations as it provides a steep travelling wave type profile for the exact solution. Solutions are obtained for the domain $-60 \leq x \leq 60$ even though Figure 6 shows only selected intervals of the domain where there are significant differences in the solutions. Figure 7 illustrates how the RMSE and computational time vary with the number of mesh points on the domain for the numerical simulations that used `pdepe.m` and FVML.

This reaction-diffusion problem is then converted to an advection-reaction-diffusion problem by adding an advection term into the equation so that the equation becomes

$$\frac{\partial T}{\partial t} = \frac{\partial^2 T}{\partial x^2} - \frac{\partial}{\partial x}(\chi T) + \frac{8}{\delta^2} T^2(1-T) + g_2(x,t); \tag{11}$$

Computational time and root mean square error in producing results of equation (10)

δt	**Computational Time (s)**				**Root Mean Squares Error**			
	$\delta x = 0.2$	$\delta x = 0.1$	$\delta x = 0.05$	$\delta x = 0.02$	$\delta x = 0.2$	$\delta x = 0.1$	$\delta x = 0.05$	$\delta x = 0.02$
(i) 0.0005	0.32813	0.625	1.2031	3.2188	0.057153	0.0031418	0.040547	0.04793
(ii) 0.0001	1.5781	2.9531	5.6406	13.9063	0.071584	0.037063	0.0013962	0.01091
(iii) 0.00005	3.1719	5.7969	11.3438	28.09	0.073417	0.040826	0.0078428	0.004412
(iv) N/A	44.8281	88.1875	177.9688	459.1	0.30402	0.16137	0.077766	0.02047

Table 1: Comparison of computational time and root mean square error for the solutions of equation (10) when $\delta = 0.1$ on the domain $-60 \leq x \leq 60$. (i), (ii) and (iii) - FVML with $\delta t = 0.0005$, 0.0001 and 0.00005 respectively. (iv) - `pdepe.m`. The values for (ii) are relevant to the results shown in Figure 6.

where $g_2(x,t) = \chi \dfrac{\partial \hat{T}}{\partial x}$ is an explicit function of x and t, in order to analyse the stability of the FVML technique discussed here. The parameter χ is used to switch from the original problem ($\chi = 0$) to the modified problem ($\chi = 1$) and vice versa. This advection-reaction-diffusion problem still satisfies the exact solution $T(x,t) = \hat{T}(x,t)$ given above according to the concept of method of manufactured solutions. Figure 8 illustrates how the RMSE and the computational time vary with the number of mesh points on the domain for the numerical simulations that used `pdepe.m` and FVML for this modified problem.

Figures 7 and 8 depict how FVML keeps the stability of the solutions when the time step or the space step are changed. It is obvious that the computational times required for extremely small time step sizes for FVML are higher than the computational times taken by pdepe.m when it runs on the same computational meshes where pdepe.m does not change time step size. It is also worthwhile to note that the accuracy achieved by FVML has always been better than pdepe.m except for the case where FVML has used a large time step size.

3.3. Code verification using the method of manufactured solutions for an ARD problem

Here we consider the partial differential equation model discussed in the sub section 3.4 for the purpose of constructing a new advection–reaction–diffusion model that has the manufactured solutions

$$u = \hat{u}(x,t) = \frac{\chi^2}{\chi^2 + exp(\chi(x - x_0 - t))}$$

and

$$c = \hat{c}(x,t) = 1 - 0.5\hat{u}.$$

These solutions are chosen considering the expected behaviour of the solutions of the model considered in that example. Using the method discussed in [13], [14] and [15] it is easy to verify

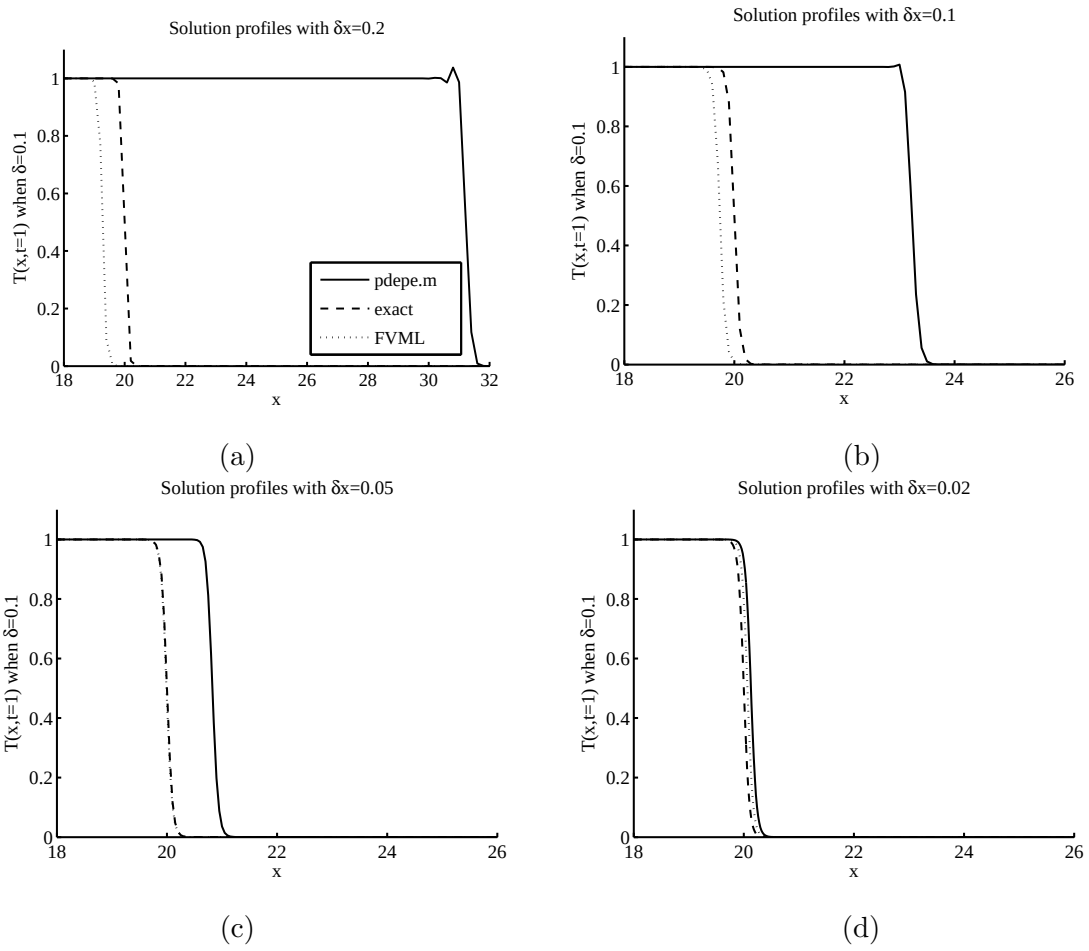

Figure 6: Solutions of the equation (10) when $\delta = 0.1$ at time $t = 1$: dotted line - using finite volume technique discussed here with $\delta t = 0.0001$, thick line - using `pdepe.m` and dashed line - exact solution.

that $u = \hat{u}(x,t)$ and $c = \hat{c}(x,t)$ are solutions for the new model described by

$$\frac{\partial u}{\partial t} - \frac{\partial^2 u}{\partial x^2} + \frac{\partial}{\partial x}\left(u\chi\frac{\partial c}{\partial x}\right) - u(1-u) = f_1(x,t) \tag{12}$$

$$\frac{\partial c}{\partial t} - 1 + c + uc = f_2(x,t) \tag{13}$$

where

$$f_1(x,t) = \frac{\partial \hat{u}}{\partial t} - \frac{\partial^2 \hat{u}}{\partial x^2} + \frac{\partial}{\partial x}\left(\hat{u}\chi\frac{\partial \hat{c}}{\partial x}\right) - \hat{u}(1-\hat{u})$$

and

$$f_2(x,t) = \frac{\partial \hat{c}}{\partial t} - 1 + \hat{c} + \hat{u}\hat{c}.$$

Now the solutions of the equations (12) and (13) with compatible initial conditions ($u(x,0) = \hat{u}(x,0)$ and $c(x,0) = \hat{c}(x,0)$ for $0 \le x \le 1$) and boundary conditions ($u(0,t) = \hat{u}(0,t)$, $c(0,t) = \hat{c}(0,t)$, $u(L,t) = \hat{u}(L,t)$ and $c(L,t) = \hat{c}(L,t)$ for $t > 0$) will be $u = \hat{u}(x,t)$ and $c = \hat{c}(x,t)$.

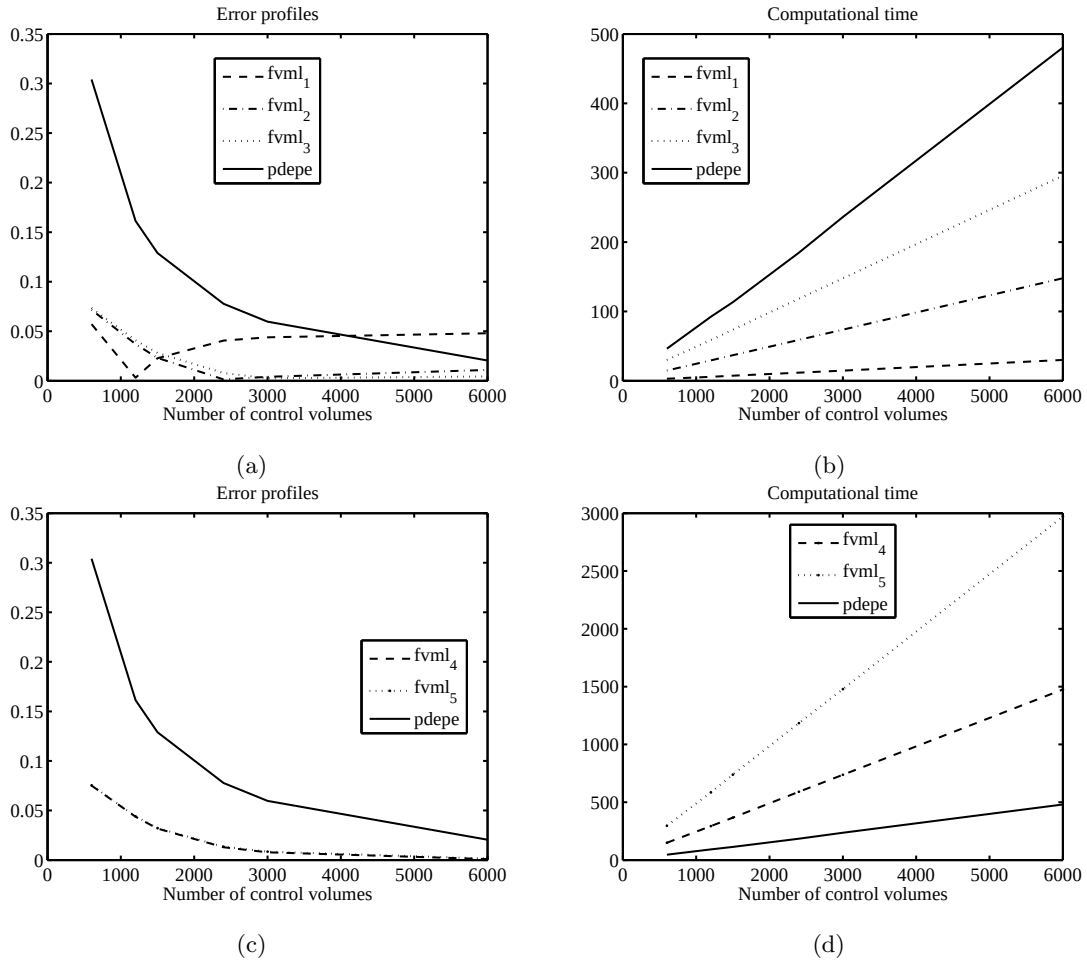

Figure 7: *Comparison of RMSE and computational time required for solving equation (10) using FVML and* `pdepe.m` *codes when* $\delta = 0.1$ *on the domain* $-60 \leq x \leq 60$. *(a) RMSE and (b) computational time calculated for simulations by* `pdepe.m` *and FVML for different time step sizes (*$fvml_1$*:* $\delta t = 0.0005$, $fvml_2$*:*$\delta t = 0.0001$, $fvml_3$*:*$\delta t = 0.00005$*). Similarly (c) and (d) again provide RMSE and computational time for* `pdepe.m` *and FVML (*$fvml_4$*:* $\delta t = 0.00001$, $fvml_5$*:* $\delta t = 0.000005$*)*

The numerical solutions and exact solutions of this constructed model are compared in Figure 9 for verifying the code which uses the proposed finite volume technique incorporating an approach to treat the nonlinear source term.

3.4. Diffusive and chemotactic cellular migration

A mathematical model describing cell migration by diffusion and chemotaxis given by equations

$$\frac{\partial u}{\partial t} = D_u \frac{\partial^2 u}{\partial x^2} - \frac{\partial}{\partial x}\left(u\chi \frac{\partial c}{\partial x}\right) + u(1-u) \tag{14}$$

$$\frac{\partial c}{\partial t} = 1 - c - uc \tag{15}$$

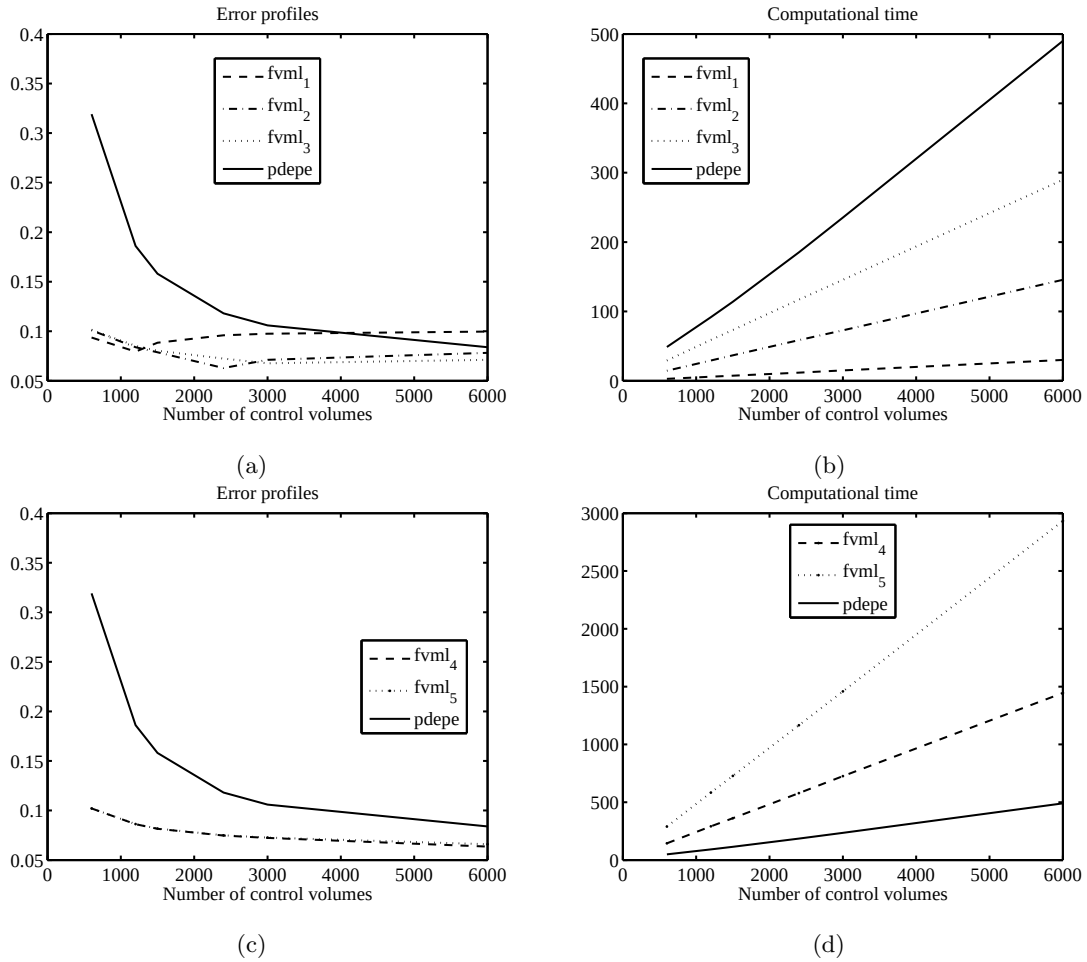

Figure 8: *Comparison of RMSE and computational time required for solving equation (11) using FVML and* `pdepe.m` *codes when* $\delta = 0.1$ *on the domain* $-60 \leq x \leq 60$. *(a) RMSE and (b) computational time calculated for simulations by* `pdepe.m` *and FVML for different time step sizes (*$fvml_1$*:* $\delta t = 0.0005$*,* $fvml_2$*:*$\delta t = 0.0001$*,* $fvml_3$*:*$\delta t = 0.00005$*). Similarly (c) and (d) again provide RMSE and computational time for* `pdepe.m` *and FVML (*$fvml_4$*:* $\delta t = 0.00001$*,* $fvml_5$*:* $\delta t = 0.000005$*)*

has been considered in [5] for a number of different constant χ and D_u values, with zero flux boundary conditions and initial conditions given by

$$u(x,0) = \begin{cases} 1 & x < 10 \\ e^{-\zeta(x-10)} & x \geq 0\,, \end{cases}$$

$$c(x,0) = 1.0 \text{ for } 0 \leq x \leq L.$$

Travelling wave solutions with constant wave speed have been obtained in [5], demonstrating the onset of shock-like wavefronts with increasing chemotactic sensitivity χ. In order to capture the shock front, Landman *et al.* [5] separate the model into distinct hyperbolic and parabolic parts (operator splitting) and employ a front tracking and smoothing algorithm with

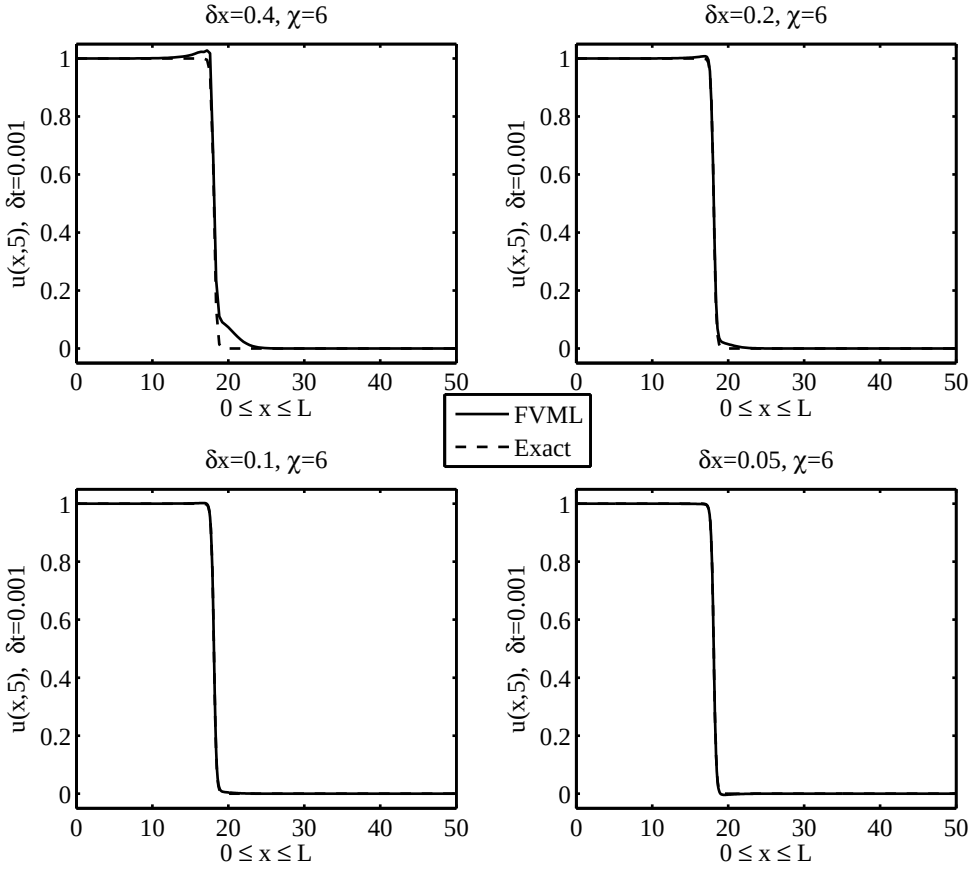

Figure 9: Comparison of numerical solutions (solid line) obtained by proposed method and exact solutions (dashed line) for the function u of equations (12) and (13) on $0 \leq x \leq 50$ after $5s$ with $\delta t = 0.001$ and $\chi = 6$.

a dependency on very small time steps for the hyperbolic component.

In contrast to the complexity of such a scheme we show here solutions of the same problem, where no smoothing at the front has been employed, relying only on our direct finite volume discretisation of the governing equations. Figure 10 displays the solutions for a number of choices of the the parameter χ and parameter D_u with $\zeta = 10$ using the initial conditions given above. These results in Figure 10(a) and 10(b), which were obtained with the same parameter values as in [5], are highly comparable with the simulations provided in [5] demonstrating the adaptability of our scheme for degenerate parabolic systems. Figure 10(c) and 10(d) show the result of MATLAB code `pdepe.m` which fails to cope with very high values of χ (50 and 100) and very low values of D_u (0 and 0.1 near $x = 0$) respectively.

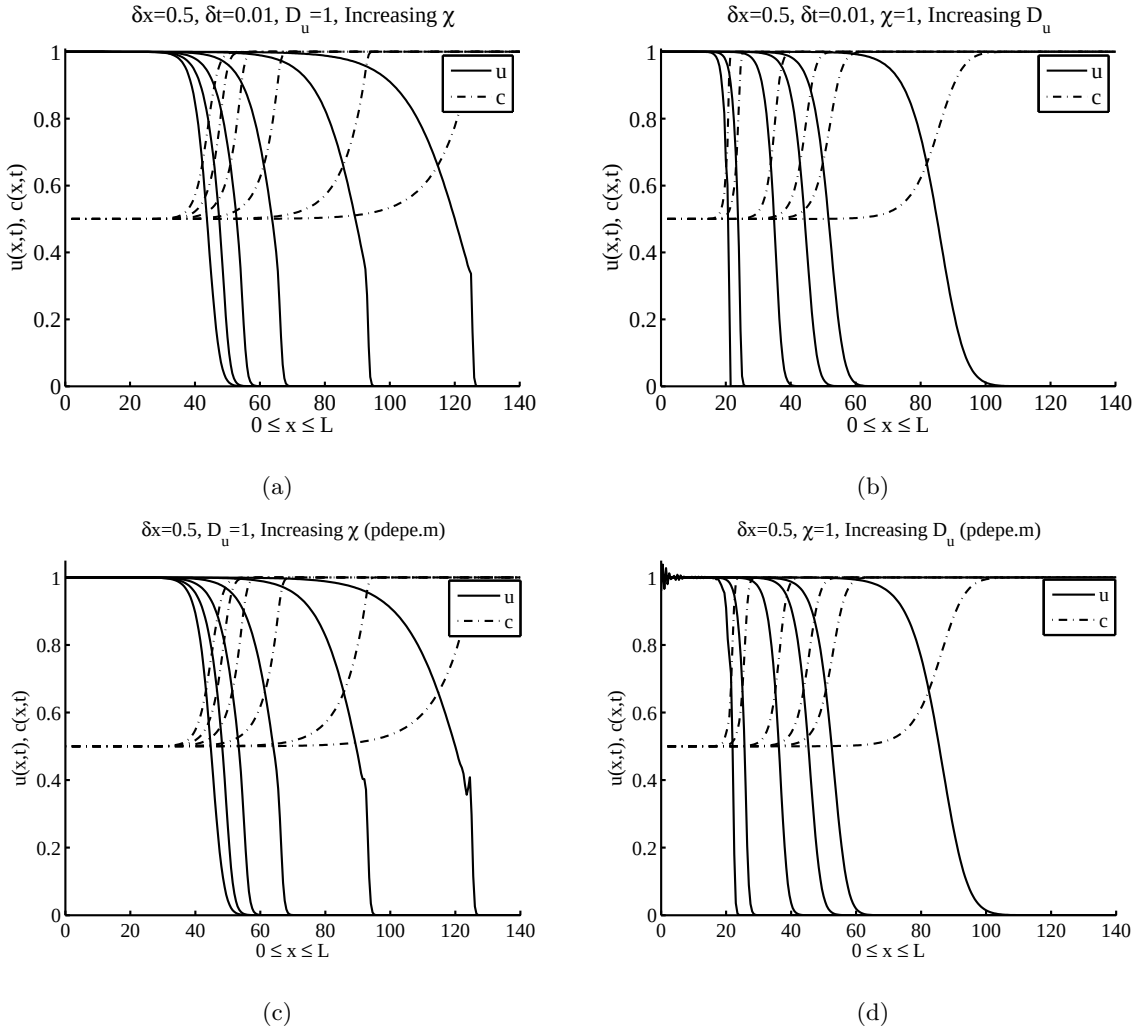

Figure 10: Graphs of $u(x, 20)$ and $c(x, 20)$ obtained using the proposed finite volume method (see (a) and (b)) and `pdepe.m` (see (c) and (d)) for the solution of equations (14)-(15): (a) and (c): The influence of increasing chemotaxis χ from left to right with values 0, 5, 10, 20, 50, 100 for fixed $D_u = 1$. (b) and (d): The influence of increasing diffusion (D_u) from left to right with values 0, 0.1, 0.5, 1.0, 1.5, 5.0 when $\chi = 1$ fixed. Note that $\delta t = 0.01$ was fixed throughout the computation for simulations in (a) and (b).

3.5. A model of wound healing angiogenesis in soft tissue

The ingrowth of tissue into a thin, disc-like wound chamber within the dermis has been discussed in [16] as a initial boundary value problem which consists of three governing equations with diffusion, advection and reaction terms. The governing equations for capillary tip density $n(x, t)$, chemoattractant concentration $a(x, t)$ and blood vessel density $b(x, t)$ had been non–dimensionalised to arrive at the following equations with given initial and boundary conditions below.

Equations:

$$\frac{\partial n}{\partial t} = \mu_n \frac{\partial^2 n}{\partial x^2} - \chi \frac{\partial}{\partial x}\left(n \frac{\partial a}{\partial x}\right) + \lambda_1 ab - \lambda_2 n - \lambda_0 n^2 \tag{16}$$

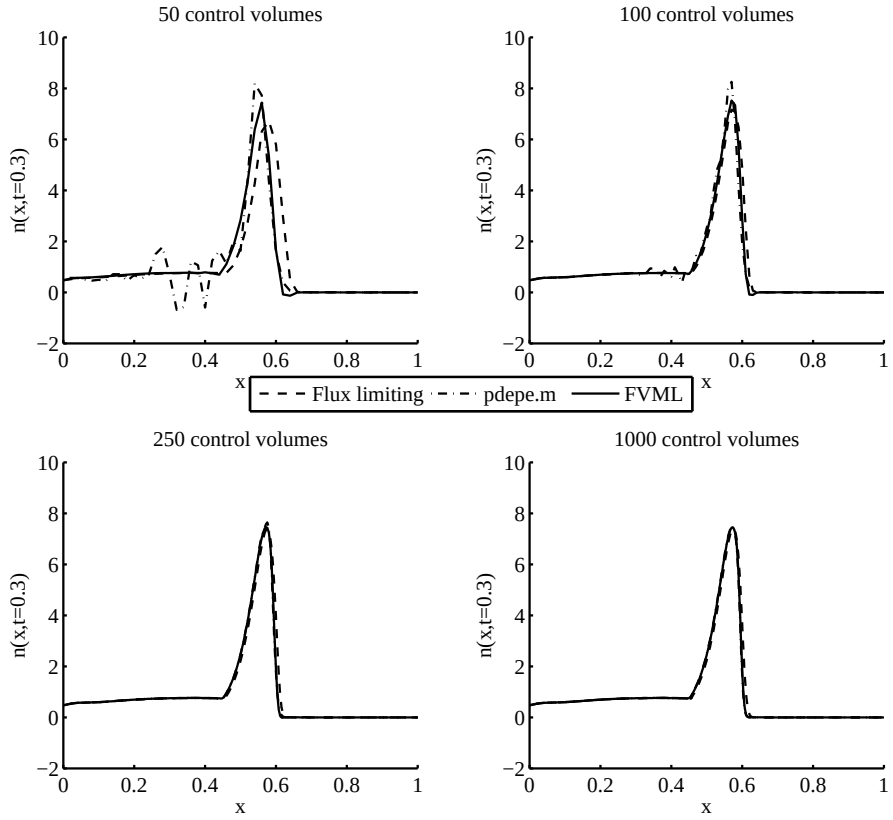

Figure 11: The comparison of the numerical results for equations (16)–(18) by the proposed method and flux limiting approach with $\delta t = 0.0005$ and `pdepde.m`.

$$\frac{\partial a}{\partial t} = D\frac{\partial^2 a}{\partial x^2} + \frac{\lambda_4}{2}\left[1 + \tanh\left(\frac{1-b}{\delta}\right)\right] - \lambda_4 a - \lambda_5 ab \tag{17}$$

$$\frac{\partial b}{\partial t} = \mu_b \frac{\partial}{\partial x}\left(n\frac{\partial b}{\partial x}\right) - \mu_n \frac{\partial n}{\partial x} + \chi n \frac{\partial a}{\partial x} \tag{18}$$

Boundary conditions:

$$n(0,t) = \hat{n}e^{-\alpha_1 t}, \quad \frac{\partial a}{\partial x}(0,t) = \lambda_7 a(0,t)\hat{b}, \quad b(0,t) = \hat{b},$$

and

$$\frac{\partial n}{\partial x}(1,t) = \frac{\partial a}{\partial x}(1,t) = \frac{\partial b}{\partial x}(1,t) = 0 \quad \text{for} \quad t > 0.$$

Initial conditions:

$$n(x,0) = \begin{cases} \dfrac{\hat{n}}{\bar{x}^3}(x-\bar{x})(2x^2 - \bar{x}x - \bar{x}^2) & \text{for } x \in [0,\bar{x}) \\ 0 & \text{for } x \in [\bar{x},1] \end{cases}$$

$$a(x,0) = 0 \quad \forall x \in [0,1]$$

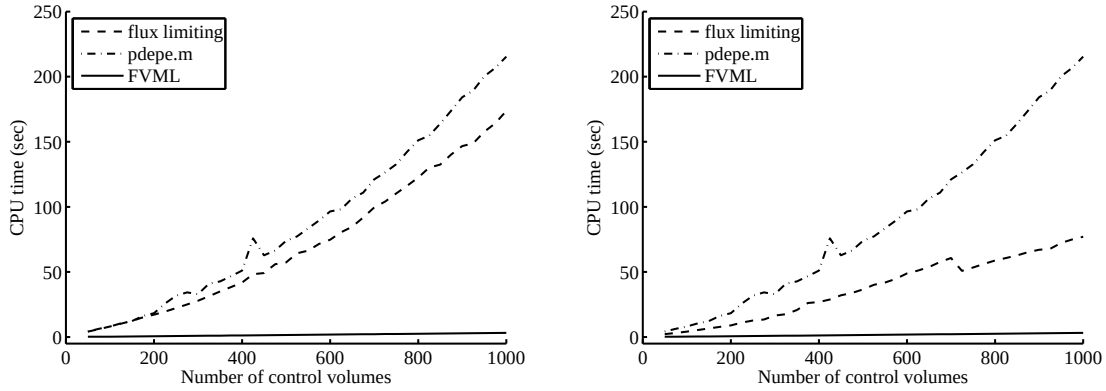

(a) (b)

Figure 12: The comparison of computational time (in seconds) taken for producing the numerical results for equations (16)–(18) by the proposed method (FVML), flux limiting approach and `pdepde.m`. Figures (a) and (b) show the computational time taken when $\delta t = 0.0005$ and $\delta t = 0.001$ are used respectively. Note that δt value for the `pdepe.m` is not known.

$$b(x,0) = \begin{cases} \bar{b} + \dfrac{\hat{b} - \bar{b}}{\bar{x}^3}(x - \bar{x})(2x^2 - \bar{x}x - \bar{x}^2) & \text{for } x \in [0, \bar{x}) \\ \bar{b} & \text{for } x \in [\bar{x}, 1] \end{cases}$$

The finite volume technique discussed in this paper avoids the requirement of solving a nonlinear system of equations which typically arise with traditional discretisation procedures for this type of PDE system.

Figure 11 shows the relevant results with parameter values $\mu_n = 0.001$, $\mu_b = 0.001$, $D = 1$, $\chi = 1.5$, $\lambda_0 = 3$, $\lambda_1 = 100$, $\lambda_2 = 1$, $\lambda_4 = 100$, $\lambda_5 = 10$, $\lambda_7 = 10$, $\alpha_1 = 2.5$ $\delta = 0.01$, $\hat{n} = 1$, $\hat{b} = 1.5$, $\bar{b} = 0.0$ and $\bar{x} = 0.05$ as used in [4]. The results obtained using the proposed method (solid lines) are highly comparable with those obtained in [4] using the finite volume method with a van Leer flux limiting approach (dashed lines). Figure 11 also displays the numerical oscillations of the solutions obtained using MATLAB's `pdepe.m` code to solve the problem (dash-dot lines). Figure 12 provides comparisons of the computational time for obtaining the numerical solutions using a flux limiting technique (dashed lines) and MATLAB's `pdepe.m` (dash-dot lines) discussed in [4] and proposed finite volume method with linearisation of source term (solid lines) for two time step sizes $\delta t = 0.0005$ and $\delta t = 0.001$. This provides a strong evidence for the low computational cost required for the numerical simulations of PDE models with nonlinear source terms when the proposed method is used. Figure 13 provides solutions of FMVL for the function n at different time levels with $\delta x = 0.0002$ and $\delta t = 0.0001$. In addition to that Figure 13 depicts how the absolute value of the MBE, which is a measure of error in spatial discretisation for the function $n(x,t)$, changes as the number of control volumes

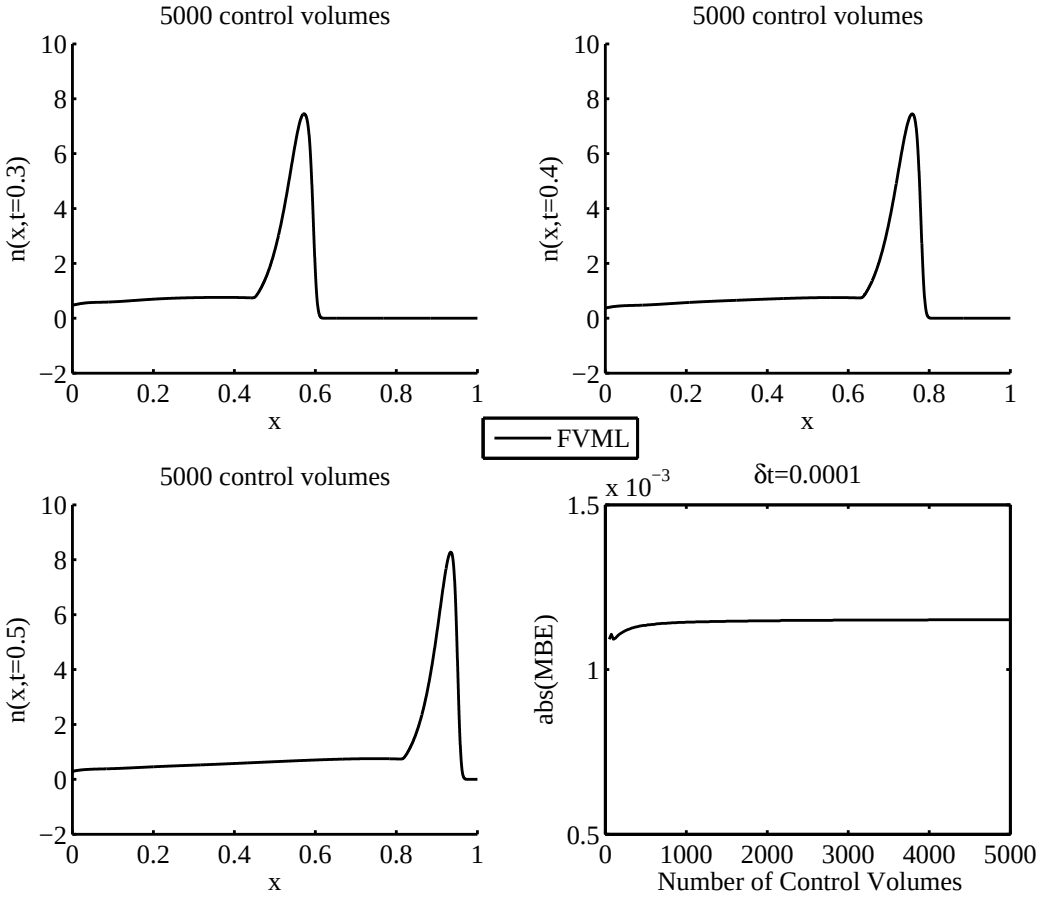

Figure 13: The plots for the function $n(x,t)$ of equation (16) at time $t = 0.3$, $t = 0.4$ and $t = 0.5$ obtained using FVML with 5000 control volumes and $\delta t = 0.0001$ as the time step and the plot of the absolute value of the error measurement MBE as δx decreases when $\delta t = 0.0001$ for the numerical solutions for the function n of equation (16) using FVML.

increases for the numerical simulation of the above model given by the equations (16)–(18) using the proposed method. These results together with the results obtained in the previous sections provide a strong evidence on the stability and the convergence of the method proposed.

4. Discussion

We are interested here in problems modelled as advection–reaction–diffusion systems in one spatial dimension where the particular distinguishing characteristic is the need to find numerical solutions when small limit approximations are not appropriate for the advective, reactive or diffusive components, individually or in combination.

We have shown in this article just how we have constructed a method of solution even in the neighbourhood of small limits, that captures to a broad variety of diffusive and tactically driven

processes modelled in the literature. Many of these problems describe, particularly at the small diffusion limit, shock-like fronts to travelling wave solutions and typical numerical methods employed to generate these make use of computationally expensive smoothing or flux-limiting techniques at the shock front.

In our exploration of advection–reaction–diffusion systems in one spatial dimension, particularly those where the advective and reaction components are of a similar order, and the reactions are nonlinear, we have recognised that the reaction terms can make a significant contribution to solution error at the steep front. For this reason we have focused here on the solution of strongly advective problems, eschewing any front smoothing or flux limiting to show that the use of a higher order up–winding scheme combined with an appropriate linearisation in time for the nonlinear reaction terms provides solutions of high accuracy. The increased accuracy of this approach is best seen by comparing our results with those of Landman *et al.* [5] and the flux-limiting approach adopted by Thackham *et al.* [4].

It would seem natural from the perspective adopted here that the use of both a high order upwinding scheme and linearisation in time provides an accurate method that could easily be adapted to include a smoothing algorithm in the neighbourhood of shock fronts, providing a reliable numerical scheme capable of rendering accurate solutions for a wide range of Péclet and Damköhler numbers, covering a wide range of advection–diffusion–reaction models of interest in the bio–mathematical community.

Acknowledgments. The authors wish to acknowledge the support provided by the Australian Research Council in the partial funding of this work from grant DP0773230. The authors also wish to thank Jennifer A. Thackham, the corresponding author of the article [4], for providing the MATLAB codes for producing numerical solutions of equations (16)–(18) using the finite volume method with flux limiting.

Appendix

The following equations represent the coefficients associated with the *FVML* scheme introduced in this article and summarized in equation (5) in Section 2.4.

$$
\begin{aligned}
p_{i-2} =& -b_{i-2}\chi(C_{iw}^{(j+1)})\left(C_i^{(j+1)} - C_{i-1}^{(j+1)}\right)(1-\alpha)\frac{\delta t}{\delta x^2} \\
p_{i-1} =& \left[-D_u + a_{i-1}\chi(C_{ie}^{(j+1)})\left(C_{i+1}^{(j+1)} - C_i^{(j+1)}\right) - b_{i-1}\chi(C_{iw}^{(j+1)})\left(C_i^{(j+1)} - C_{i-1}^{(j+1)}\right)\right](1-\alpha)\frac{\delta t}{\delta x^2} \\
&+ \frac{1}{24} - \frac{\delta t}{24}\bar{f}_1(U_{i-1}^{(j)}, C_{i-1}^{(j)}, C_{i-1}^{(j+1)}, \beta) \\
p_i =& \left[2D_u + a_i\chi(C_{ie}^{(j+1)})\left(C_{i+1}^{(j+1)} - C_i^{(j+1)}\right) - b_i\chi(C_{iw}^{(j+1)})\left(C_i^{(j+1)} - C_{i-1}^{(j+1)}\right)\right](1-\alpha)\frac{\delta t}{\delta x^2} \\
&+ \frac{22}{24} - \frac{22\delta t}{24}\bar{f}_1(U_i^{(j)}, C_i^{(j)}, C_i^{(j+1)}, \beta) \\
p_{i+1} =& \left[-D_u + a_{i+1}\chi(C_{ie}^{(j+1)})\left(C_{i+1}^{(j+1)} - C_i^{(j+1)}\right) - b_{i+1}\chi(C_{iw}^{(j+1)})\left(C_i^{(j+1)} - C_{i-1}^{(j+1)}\right)\right](1-\alpha)\frac{\delta t}{\delta x^2} \\
&+ \frac{1}{24} - \frac{\delta t}{24}\bar{f}_1(U_{i+1}^{(j)}, C_{i+1}^{(j)}, C_{i+1}^{(j+1)}, \beta) \\
p_{i+2} =& a_{i+2}\chi(C_{ie}^{(j+1)})\left(C_{i+1}^{(j+1)} - C_i^{(j+1)}\right)(1-\alpha)\frac{\delta t}{\delta x^2}
\end{aligned}
$$

$$
\begin{aligned}
q_{i-2} =& b_{i-2}\chi(C_{iw}^{(j)})\left(C_i^{(j)} - C_{i-1}^{(j)}\right)\frac{\alpha\delta t}{\delta x^2} \\
q_{i-1} =& \left[D_u - a_{i-1}\chi(C_{ie}^{(j)})\left(C_{i+1}^{(j)} - C_i^{(j)}\right) + b_{i-1}\chi(C_{iw}^{(j)})\left(C_i^{(j)} - C_{i-1}^{(j)}\right)\right]\frac{\alpha\delta t}{\delta x^2} + \frac{1}{24} \\
q_i =& \left[-2D_u - a_i\chi(C_{ie}^{(j)})\left(C_{i+1}^{(j)} - C_i^{(j)}\right) + b_i\chi(C_{iw}^{(j)})\left(C_i^{(j)} - C_{i-1}^{(j)}\right)\right]\frac{\alpha\delta t}{\delta x^2} + \frac{22}{24} \\
q_{i+1} =& \left[D_u - a_{i+1}\chi(C_{ie}^{(j)})\left(C_{i+1}^{(j)} - C_i^{(j)}\right) + b_{i+1}\chi(C_{iw}^{(j)})\left(C_i^{(j)} - C_{i-1}^{(j)}\right)\right]\frac{\alpha\delta t}{\delta x^2} + \frac{1}{24} \\
q_{i+2} =& -a_{i+2}\chi(C_{ie}^{(j+1)})\left(C_{i+1}^{(j+1)} - C_i^{(j+1)}\right)\frac{\alpha\delta t}{\delta x^2}
\end{aligned}
$$

$$
\begin{aligned}
r_{i-1} =& \frac{\delta t}{24}\bar{f}_2(U_{i-1}^{(j)}, C_{i-1}^{(j)}, C_{i-1}^{(j+1)}, \beta) \\
r_i =& \frac{22\delta t}{24}\bar{f}_2(U_i^{(j)}, C_i^{(j)}, C_i^{(j+1)}, \beta) \\
r_{i+1} =& \frac{\delta t}{24}\bar{f}_2(U_{i+1}^{(j)}, C_{i+1}^{(j)}, C_{i+1}^{(j+1)}, \beta)
\end{aligned}
$$

References

[1] A. R. A. Anderson, M. A. J. Chaplain, E. L. Newman, R. J. C. Steele and A. M. Thompson, *Mathematical modelling of tumour invasion and metastasis*, Journal of Theoretical Medicine, 2 (2000) 129–154.

[2] K. Painter, *Continuous Models for Cell Migration in Tissues and Applications to Cell Sorting via Differential Chemotaxis*, Bulletin of Mathematical Biology, 71(5) (2009) 1117–1147.

[3] Shigeru Kondo and Takashi Miura, *Reaction-Diffusion Model as a Framework for Understanding Biological Pattern Formation*, Science, 329(5999) (2010) 1616–1620.

[4] Jennifer A. Thackham, D. L. Sean McElwain, Ian W. Turner, *Computational approaches to solving equations arising from wound healing*, Bulletin of Mathematical Biology, 71 (2009) 211–246.

[5] K. A. Landman, M. J. Simpson, J. L. Slater and D. F. Newgreen, *Diffusive and chemotactic cellular migration: smooth and discontinuous traveling wave solutions*, SIAM Journal on Applied Mathematics, 65 (4) (2005) 1420–1442.

[6] J. I. Ramos, *A finite volume method for one-dimensional reaction-diffusion problems*, Applied Mathematics and Computation, 188 (2007) 739–748.

[7] B. P. Leonard, *A stable and accurate convective modelling procedure based on quadratic upstream interpolation*, Computer Methods in Applied Mechanics and Engineering, 19 (1979) 59–98.

[8] Curtis C. Ober, John N. Shadid, *Studies on the accuracy of time-integration methods for the radiation-diffusion equations*, Journal of Computational Physics, 195 (2004) 743–772.

[9] D. A. Knoll, L. Chacon, L. G. Margolin and V. A. Mousseau, *On balanced approximations for time integration of multiple time scale systems*, Journal of Computational Physics, 185 (2003) 583–611.

[10] Kerry A. Landman, Matthew J. Simpson, Graeme J. Pettet, *Tactically-driven nonmonotone travelling waves*, Physica D: Nonlinear Phenomena, 237(5) (2008) 678–691.

[11] R. L. Burden and J. D. Faires, *Numerical Analysis (7th edition)*, PWS Publishing Company, Boston, 2001.

[12] D. G. Mallet, I. W. Turner, G. J. Pettet, *Application of the control volume method to a mathematical model of cell migration*, ANZIAM Journal, 45 (E), (2004) C891–C904.

[13] W. L. Oberkampf and C. J. Roy, *Verification and validation in scientific computing*, Cambridge University Press (2010).

[14] P. J. Roache, *Code verification by the method of manufactured solutions*, Transactions of the AMSE, 124 (2002) 4–10.

[15] W. L. Oberkampf and T. G. Trucano, *Verification and validation in computational fluid dynamics*, Progress in Aerospace Sciences, 38 (2002) 209–272.

[16] G. J. Pettet, H. M. Byrne, D. L. S. McElwain and J. Norbury, *A model of wound–healing angiogenesis in soft tissue*, Mathematical Biosciences, 136(1) (1996) 35–63.

[17] Omar M. Knio, Habib N. Najm and Peter S. Wyckoffy, *A Semi-implicit Numerical Scheme for Reacting Flow: II. Stiff, Operator-Split Formulation*, Journal of Computational Physics, 154 (1999) 428–467.